

Differentiable Iterative Surface Normal Estimation

Jan Eric Lenssen

Christian Osendorfer

Jonathan Masci

NNAISENSE, Switzerland

{janeric, christian, jonathan}@nnaisense.com

Abstract

This paper presents an end-to-end differentiable algorithm for anisotropic surface normal estimation on unstructured point-clouds. We utilize graph neural networks to iteratively infer point weights for a plane fitting algorithm applied to local neighborhoods. The approach retains the interpretability and efficiency of traditional sequential plane fitting while benefiting from a data-dependent deep-learning parameterization. This results in a state-of-the-art surface normal estimator that is robust to noise, outliers and point density variation and that preserves sharp features through anisotropic kernels and a local spatial transformer. Contrary to previous deep learning methods, the proposed approach does not require any hand-crafted features while being faster and more parameter efficient.

1. Introduction

Normal vectors are local surface descriptors that are used as an input for several computer vision tasks ranging from surface reconstruction [25] to registration [36] and segmentation [16]. For this reason, the task of surface normal estimation has been an important and well studied research topic for a long time [21], with several methods dating back up to 30 years. Progress in the field, however, has been plateauing only until recently, when a new series of works has shown that improvements are still possible with the use of data-driven deep learning techniques [4, 18, 6], as also shown in related fields like point cloud denoising [39] or finding correspondences on meshes and point clouds [9, 13, 33, 30]. Deep learning methods are known to often achieve far better results compared to data-independent methods. However, they have downsides in terms of robustness to small input changes, adversarial attacks, interpretability, and sometimes also computational efficiency. Also, they do not make use of often well-known intrinsic problem structure, which leads to the necessity of having a large amount of training data and model parameters.

In this work we explore a different route and follow

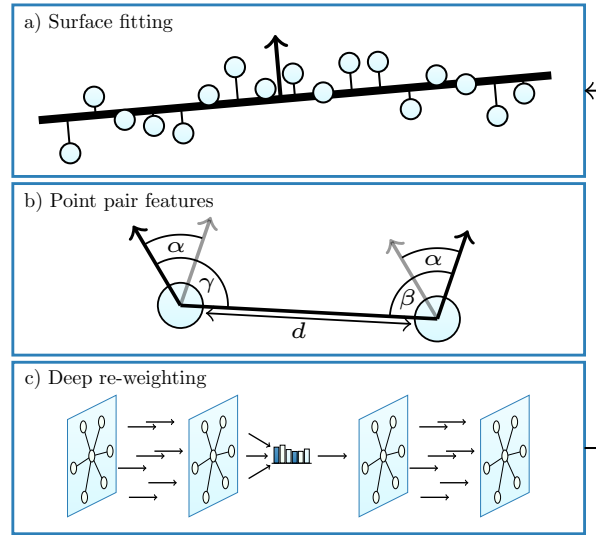


Figure 1: Overview over the proposed method for iterative surface normal estimation. (a) Surfaces are fitted by optimizing weighted least squares. (b) Intermediate surface descriptors (Point Pair Features) are computed from intermediate results and used to (c) refine the weights for the next step of the least squares fitting, using a graph neural network.

the paradigm of differentiable programming to enhance the well known sequential least squares problem with a deep data-dependent parameterization (c.f. Figure 1). The proposed algorithm attains state-of-the-art performance in surface normal estimation on unstructured point clouds, is robust, interpretable and fast. It can handle various noise levels, outliers, point density variation and preserves sharp features through the use of learned, anisotropic kernels. From a deep learning perspective, the approach leverages task-specific knowledge to impose a geometric inductive bias on the architecture. Thanks to this strong inductive bias our model complexity can be kept very low, making the approach robust and efficient.

2. Related work

Traditional methods for surface normal estimation make use of plane fitting approaches like unweighted principal component analysis (PCA) [21] and singular value decomposition (SVD) (c.f. [26] for an overview). The performance of these approaches usually hinges upon the often cumbersome selection of data-specific hyper-parameters, such as point neighborhood sizes, and it is sensitive to noise, outliers and density variations. Because of this, several heuristics have been proposed throughout the years to ease such selection, e.g. those for finding a neighborhood size of plane fitting [32]. Another limitation of plane fitting methods is that they tend to average out sharp details, in fact they can be seen as isotropic low-pass filters. In order to preserve sharp features methods that extract normal vectors from estimated Voronoi cells have been proposed [2, 31] and combined with PCA [1]. Alternative approaches include edge-aware sampling [22] or normal vector estimation in Hough space [5]. In addition, several methods arise from more complex surface reconstruction techniques like moving least squares (MLS) [28], spherical fitting [17] or jet fitting [8].

Deep learning methods. Deep learning based approaches also found their way into surface normal estimation with the recent success of deep learning in a wide range of domains. These approaches can be divided into two groups, depending on the actual type of input data they use. The first group aims at normal estimation from single images [27, 3, 11, 29, 42, 38, 14] and has received a lot of interest over the last few years due to the well understood properties of CNNs for grid-structured data.

The second line of research directly uses unstructured point clouds and emerged only very recently, partially due to the advent of graph neural networks and geometric deep learning [7]. Boulch et al. [6] proposed to use a CNN on Hough transformed point clouds in order to find surface planes of the point cloud in Hough space. Based on the recently introduced point processing network, PointNet [37], Guerrero et al. [18] proposed a deep multi-scale architecture for surface normal estimation. Later, Ben-Shabat et al. [4] improved on those results using 3D point cloud fisher vectors as input features and a three-dimensional CNN architecture consisting of experts.

Differentiable sequential least squares. Methods solving least squares problems with weights estimated by deep neural networks received increasing interest due to their vast applicability to problems such as fundamental matrix estimation [40], 3D keypoint estimation [41], and transformation synchronization [23]. Together with our approach, those methods have in common that they backpropagate gradients through SVD or eigendecomposition to utilize statistics from large datasets.

3. Background

Let \mathcal{S} be a manifold in \mathbb{R}^3 , $\mathcal{P} = \{\mathbf{p}_0, \dots, \mathbf{p}_m\}$ a finite set of sampled and possibly distorted points from that manifold and $\hat{\mathbf{N}} = \{\hat{\mathbf{n}}_0, \dots, \hat{\mathbf{n}}_m\}$ the tangent plane normal vectors at sample points \mathbf{p}_i . *Surface normal estimation* for the point cloud \mathcal{P} can be described as the problem of estimating a set of normal vectors $\mathbf{N} = \{\mathbf{n}_0, \dots, \mathbf{n}_m\}$ given \mathcal{P} , whose direction match those of the actual surface normals $\hat{\mathbf{n}}_i$ as close as possible. In this work, we mainly consider the problem of unoriented normal estimation, determining the normal vectors up to a sign flip. Estimating the correct sign can be done in a post-processing step, depending on the task at hand.

A standard approach to determine unoriented surface normals is fitting planes to the local neighborhood of every point \mathbf{p}_i [28]. Let $\mathcal{N}(i)$ denote the local neighborhood of \mathbf{p}_i , with $k_i \equiv |\mathcal{N}(i)|$. Furthermore, let $\mathcal{P}(i) \in \mathbb{R}^{k_i \times 3}$ be the matrix of centered coordinates of the points from this neighborhood, that is

$$\mathcal{P}(i)_j = \mathbf{p}_j^\top - \frac{1}{k_i} \sum_{m \in \mathcal{N}(i)} \mathbf{p}_m^\top, \quad \mathbf{p}_j \in \mathcal{N}(i). \quad (1)$$

Fitting a plane to this neighborhood is then described as finding the least squares solution of a homogeneous system of linear equations:

$$\mathbf{n}_i^* = \arg \min_{\mathbf{n}: |\mathbf{n}|=1} \|\mathcal{P}(i)\mathbf{n}\|_2^2 = \arg \min_{\mathbf{n}: |\mathbf{n}|=1} \sum_{j \in \mathcal{N}(i)} \|\mathcal{P}(i)_j \cdot \mathbf{n}\|^2 \quad (2)$$

The simple plane fitting of Eq. 2 is not robust and does not result in high-quality normal vectors: It produces accurate results only if there are no outliers in the data, which is never the case in practice. Additionally, this approach eliminates sharp details because it acts as a low-pass filter on the point cloud. Even when an isotropic radial kernel function $\theta(\|\mathcal{P}(i)_j\|)$ is used to weight points according to their distance to the local mean, fine details cannot be preserved.

Both problems can be resolved through integrating weighting functions into Eq. 2. *Sharp features can be preserved* with an *anisotropic* kernel that infers weights of point pairs based on their relative positions, i.e.:

$$\mathbf{n}_i^* = \arg \min_{\mathbf{n}: |\mathbf{n}|=1} \sum_{j \in \mathcal{N}(i)} \theta(\mathbf{p}_j - \mathbf{p}_i) \cdot \|\mathcal{P}(i)_j \cdot \mathbf{n}\|^2 \quad (3)$$

where $\theta(\cdot)$ is an anisotropic kernel, considering the full Cartesian relationship between neighboring points, instead of only their distance. *Robustness* to outliers can be achieved by another kernel that weights points according to an inlier score $s_{i,j}$. More specifically, Eq. 2 is changed to

$$\mathbf{n}_i^* = \arg \min_{\mathbf{n}: |\mathbf{n}|=1} \sum_{j \in \mathcal{N}(i)} s_{i,j} \cdot \|\mathcal{P}(i)_j \cdot \mathbf{n}\|^2, \quad (4)$$

where $s_{i,j}$ weights outliers with a low and inliers with a high score. However, in order to infer information about the outlier status of points an initial model estimation is necessary. A standard solution to this circular dependency is to formulate the problem as a sequence of weighted least-squares problems. Given the residuals \mathbf{r}^l of the least squares solution from iteration l , the solution for iteration $l + 1$ is computed as

$$\mathbf{n}_i^{l+1} = \arg \min_{\mathbf{n}: |\mathbf{n}|=1} \sum_{j \in \mathcal{N}(i)} s(\mathbf{r}_{i,j}^l) \cdot \|\mathcal{P}(i)_j \cdot \mathbf{n}\|^2. \quad (5)$$

That is, the inlier score and the estimated model are refined in an alternating fashion.

4. Iterative normal estimation

The iterative reweighting least squares formulation from Eq. 5 is already in a form that allows a robust and detail-preserving solution to be found. The core question is how to derive a good weighting function that provides the characteristics of anisotropy (Eq. 3) and inlier scoring (Eq. 4).

Because there is no a priori information about the structure of the input data, a reasonable approach is to find a weighting function through supervised learning from data. More specifically, we suggest to realize the weighting function through a deep neural network which is shared by all local neighborhoods. The resulting iterative re-weighting least squares algorithm has the following alternating steps:

$$\mathbf{w}_i^l = \omega(\mathbf{N}^{l-1}, \mathcal{P}(i), \mathbf{w}_i^{l-1}), \quad (6)$$

$$\mathbf{n}_i^l = \arg \min_{\mathbf{n}: |\mathbf{n}|=1} \sum_{j \in \mathcal{N}(i)} \mathbf{w}_{i,j}^l \|\mathcal{P}(i)_j \cdot \mathbf{n}\|^2, \quad (7)$$

where $\mathbf{w}_{i,j}^l$ denotes the j 'th element of $\mathbf{w}_i^l \in \mathbb{R}^{k_i}$. The deep anisotropic kernel network $\omega(\mathbf{N}^{l-1}, \mathcal{P}(i), \mathbf{w}_i^{l-1})$ (see Section 4.2 for a detailed description) depends on the previous estimation \mathbf{N}^l as well as relative point positions $\mathcal{P}(i)$ and so the overall model is structured to be robust as well as detail-preserving.

4.1. Efficient Normal Estimation

In every iteration of the above sequential least squares method, the plane fitting problem of Eq. 7 needs to be solved. A standard approach is to utilize the Singular Value Decomposition of the weighted matrix $\text{diag}(\sqrt{\mathbf{w}_i^l})\mathcal{P}(i)$: Let $\mathbf{U}\Sigma\mathbf{V}^T$ be its decomposition, then the column vector of \mathbf{V} corresponding to the smallest singular value is the optimal solution for the given least squares problem [20, 40]. However, n SVDs need to be solved in our scenario, one for every neighborhood, which makes this approach prohibitive. A much more efficient approach in this

Algorithm 1 Differentiable iterative normal estimation

Input:

$\mathcal{P} \in \mathbb{R}^{n \times 3}$: Point cloud

L : Number of iterations

k or r : Neighborhood size (num. neighbors or radius)

Output:

$\mathbf{N} \in \mathbb{R}^{n \times 3}$: Normal vector estimations

$\mathcal{N}(i)$'s \leftarrow Neighborhood graph from \mathcal{P} and k / r

for $i \in \{1, \dots, n\}$ **in parallel do**

 Compute $\mathcal{P}(i) \in \mathbb{R}^{k_i \times 3}$

$\mathbf{w}_i^0 \leftarrow \frac{1}{k_i}$

$\mathbf{C}_i \leftarrow \mathcal{P}(i)^\top \text{diag}(\mathbf{w}_i^0)\mathcal{P}(i)$

$\mathbf{U}_i, \Sigma_i \leftarrow \text{eig}(\mathbf{C}_i)$

$\mathbf{N}_i^0 \leftarrow$ Extract \mathbf{n}_i 's from \mathbf{U}_i 's

for $l \in \{1, \dots, L\}$ **do**

$\mathbf{w}_i^l \leftarrow \omega(\mathbf{N}^{l-1}, \mathcal{P}(i), \mathbf{w}_i^{l-1})_i$

$\mathbf{C}_i \leftarrow \mathcal{P}(i)^\top \text{diag}(\mathbf{w}_i^l)\mathcal{P}(i)$

$\mathbf{U}_i, \Sigma_i \leftarrow \text{eig}(\mathbf{C}_i)$

$\mathbf{N}_i^l \leftarrow$ Extract \mathbf{n}_i from \mathbf{U}_i

end for

end for

return \mathbf{N}^L

case is to consider the eigendecomposition of the 3×3 covariance matrix $\mathbf{C}(i) = \mathcal{P}(i)^\top \text{diag}(\mathbf{w}_i^l)\mathcal{P}(i)$ which has the columns of \mathbf{V} as its eigenvectors [20]. The solution for Eq. 7 is then the eigenvector associated with the smallest eigenvalue. The computational complexity for the eigendecomposition of this 3×3 matrix is $O(1)$ and hence for one overall iteration $O(n)$.

The core algorithm can now be formulated as in Algorithm 1. The initial weighting of the points in a neighborhood is chosen to be uniform, which results in unweighted least-squares plane fitting in the initial iteration.

4.2. Deep anisotropic kernel network

Given a neighborhood $\mathcal{N}(i)$, the anisotropic kernel network infers a weight for every point in $\mathcal{N}(i)$. For the whole point cloud, this is a weight for each edge in the neighborhood graph, which is why graph neural networks [19, 12] are a natural fit. The network must be invariant to the ordering of the points in a neighborhood and it must be able to allow weight sharing over neighborhoods with varying cardinality. The proposed network architecture is outlined in Figure 2. It consists of two stages: In the first stage we compute a feature vector for each neighborhood, which is interpreted as a tuple $\mathbf{f}(i) = (\mathbf{f}^{\text{par}}(i), \mathbf{q}_i)$. Here, \mathbf{q}_i is a quaternion that parameterizes a local spatial transformer [24], given as rotation matrix $\mathbf{R}(\mathbf{q}_i)$, which normalizes local neighborhood

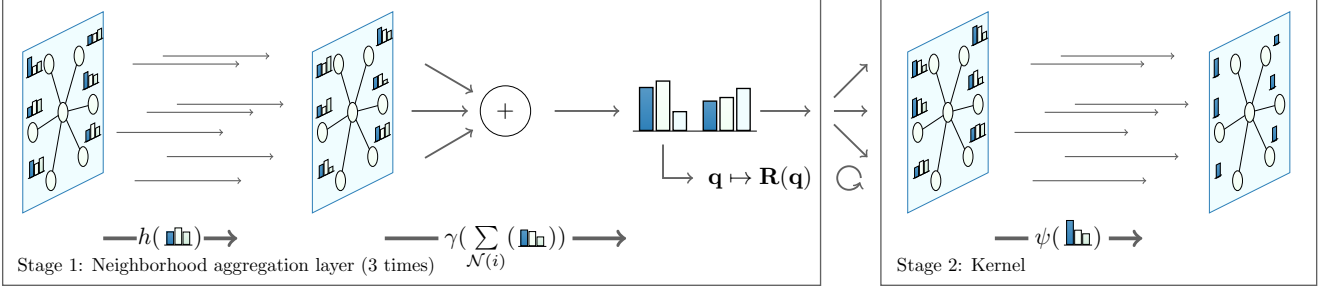


Figure 2: Neural network architecture for re-weighting of points in one neighborhood. The network consists of a neighborhood aggregation module (depicted on the left side of the figure) and the actual weighting MLP ψ (to the right of the figure). The neighborhood aggregation scheme is applied three consecutive times. The output feature vector is used to parameterize a local spatial transformer $\mathbf{R}(\mathbf{q})$ and a kernel function for the neighborhood. Then, weights for each edge are computed using the kernel MLP ψ on the kernel parameterization and the rotated positions as inputs.

orientations¹. The second stage then computes the edge weights, one for each sample j in each neighborhood $\mathcal{N}(i)$:

$$\mathbf{w}_{i,j} := \text{softmax}_{j \in \mathcal{N}(i)}(\psi(\mathbf{f}_{\mathcal{N}(i)}^{\text{par}} \parallel \mathbf{R}(\mathbf{q}_{\mathcal{N}(i)})(\mathbf{p}_j - \mathbf{p}_i))), \quad (8)$$

where \parallel denotes vector concatenation, ψ is a fully-connected network (MLP) and the feature vector $\mathbf{f}^{\text{par}}(i)$ serves as the kernel parameterization.

The first stage of the network consists of a neighborhood aggregation procedure, which is applied three consecutive times. Given MLPs h and γ , the neighborhood aggregation scheme, similar to that of PointNet [37] and to general graph neural network frameworks [19, 34], is given by

$$\mathbf{f}_e^{\text{out}}(i, j) = h(\mathbf{f}_e^{\text{in}}(i, j) \parallel \mathbf{d}_{i,j} \parallel \mathbf{ppf}(i, j)), \quad (9)$$

$$\mathbf{f}(i) = \gamma\left(\frac{1}{|\mathcal{N}(i)|} \sum_{j \in \mathcal{N}(i)} \mathbf{f}_e^{\text{out}}(i, j)\right), \quad (10)$$

where we alternate between computing new edge features and node features. In addition to the Cartesian relation vector $\mathbf{d}_{i,j} = (\mathbf{p}_j - \mathbf{p}_i)$, we utilize the idea of Point Pair Features (PPF) as proposed by Deng et al. [9, 10] (c.f. Figure 1). They are a natural fit since they use normal-based, angular input features defined as

$$\mathbf{ppf}(i, j) = (\angle(\mathbf{n}_i, \mathbf{d}_{i,j}), \angle(\mathbf{n}_j, \mathbf{d}_{i,j}), \angle(\mathbf{n}_i, \mathbf{n}_j), \|\mathbf{d}_{i,j}\|_2^2), \quad (11)$$

where we chose to compute the individual features as non-normalized cosine angles:

$$\angle(\mathbf{v}_1, \mathbf{v}_2) = |\mathbf{v}_1 \cdot \mathbf{v}_2|. \quad (12)$$

Therefore, the edge input features can be computed directly from our intermediate model estimation and directly contain the residuals of the previous least squares solution as

¹Using a rotation matrix instead of an arbitrary 3×3 matrix heavily improves training stability, also see e.g. Guerrero et al. [18].

point-plane distances $\angle(\mathbf{n}, \mathbf{d})$. After each layer, we recover new input edge features $\mathbf{f}_e^{\text{in}}(i, j) = (\mathbf{f}_e^{\text{out}}(i, j) \parallel \mathbf{f}(i))$ as a concatenation of the previous edge features and the output of the previous layer. In the first layer $\mathbf{f}_e^{\text{in}}(i, j)$ is omitted. It should be noted that this scheme leads to a constant receptive field size in the neighborhood graph that does not increase after applying one layer.

4.3. Backpropagation through eigendecomposition

Our network is trained by minimizing the distance between ground truth normals and the least squares solution, requiring backpropagation through the eigendecomposition. We follow the work of Giles [15]: Given partial derivatives $\partial L / \partial \mathbf{U}$ and $\partial L / \partial \Sigma$ for eigenvectors and eigenvalues, respectively, we compute the partial derivatives for a real symmetric 3×3 covariance matrix \mathbf{C} as

$$\frac{\partial L}{\partial \mathbf{C}} = \mathbf{U} \left(\left(\frac{\partial L}{\partial \Sigma} \right)_{\text{diag}} + \mathbf{F} \circ \mathbf{U}^\top \frac{\partial L}{\partial \mathbf{U}} \right) \mathbf{U}^\top, \quad (13)$$

where $\mathbf{F}_{i,j} = (\lambda_j - \lambda_i)^{-1}$ contains inverse eigenvalue differences. We implemented our own forward and backward steps for eigendecomposition of a large number of symmetric 3×3 matrices, where we parallelize over the neighborhoods of the point cloud, leading to an $O(1)$ implementation (using $O(n)$ processors) of parallel least squares solvers.

Handling numerical instability. Backpropagation through the eigendecomposition can lead to numerical instabilities due to at least two reasons: 1) Low-rank input matrices with two or more zero eigenvalues. 2) Exploding gradients when two eigenvalues are very close to each other and values of \mathbf{F} go to infinity. We apply two tricks to avoid these problems. First, a small amount of noise is added to the diagonal elements of all covariance matrices, making them full-rank. Second, gradients are clipped after the backward step on very large values, to tackle the cases of nearly equal eigenvalues that lead to exploding gradients.

	Ours ($k = 64$)	Nesti-Net [4]	PCPNet [18]	HoughCNN [6]	PCA	Jet [8]
No noise	6.72	6.99	9.68	10.23	12.29	12.23
Noise ($\sigma = 0.00125$)	9.95	10.11	11.46	11.62	12.87	12.84
Noise ($\sigma = 0.006$)	17.18	17.63	18.26	22.66	18.38	18.33
Noise ($\sigma = 0.012$)	21.96	22.28	22.8	33.39	27.5	27.68
Density (Stripes)	7.73	8.47	11.74	12.47	13.66	13.39
Density (Gradients)	7.51	9.00	13.42	11.02	12.81	13.13
Average	11.84	12.41	14.56	16.9	16.25	16.29

Table 1: Results for unoriented normal estimation. Shown are normal estimation errors in angle RMSE. For PCA and Jet, optimal neighborhood size for average error is chosen. For our approach, we display results for a balanced neighborhood size $k = 64$, which improves on the state of the art for all noise levels. Results for different k are shown in Table 2.

4.4. Training

Training is performed by minimizing the Euclidean distance between estimated normals $\hat{\mathbf{N}}$ and ground truth normals \mathbf{N} , averaged over all normal vectors in the training set:

$$L(\hat{\mathbf{N}}, \mathbf{N}) = \frac{1}{n} \sum_{i=1}^n \min(\|\hat{\mathbf{n}}_i - \mathbf{n}_i\|_2, \|\hat{\mathbf{n}}_i + \mathbf{n}_i\|_2), \quad (14)$$

where the minimum of the distances to the flipped or non-flipped ground truth vectors is used. While we also experimented with different angular losses, we found that the Euclidean distance loss still provides the best result and the most stable training. Similar to Ranftl and Koltun [40], a loss is computed after each least squares step. Also, we train the network iteratively by performing a gradient descent step after each iteration of the algorithm.

5. Experiments

Experiments were conducted to compare the proposed Differentiable Iterative Surface Normal Estimation with state-of-the-art methods both quantitatively, measuring normal estimation accuracy, and qualitatively, on a Poisson reconstruction and on a transfer learning task. Section 5.1 introduces the dataset used to train our model whereas Section 5.2 details the used architecture and the protocol followed in our experiments. Then, qualitative (Section 5.3) and quantitative (Section 5) results are presented together with an analysis of computational complexity (Section 5.5).

5.1. PCPNet dataset

Our method is trained and validated quantitatively on the PCPNet dataset as provided by Guerrero et al. [18]. It consists of a mixture of high-resolution scans, point clouds sampled from handmade mesh surfaces and differentiable surfaces. Each point cloud consists of 100k points. We reproduce the experimental setup of [4, 18], training on the provided split containing 32 point clouds under different

levels of noise. The test set consists of six categories, containing four sets with different levels of noise (no noise, $\sigma = 0.00125$, $\sigma = 0.0065$ and $\sigma = 0.012$) and two sets with different sampling density (striped pattern and gradient pattern). The Root Mean Squared Error (RMSE) on the provided 5k points subset is used as performance metric following the protocol of related work, where the RMSE is first computed for each test point cloud before the results are averaged over all point clouds in one category. Model selection is performed using the provided validation set.

5.2. Experimental setup and architecture

The presented graph neural network was implemented using the *Pytorch Geometric* library [12]. The neural networks h , γ and ψ each consist of two linear layers, with ReLU non-linearity. A detailed description of the architecture is presented in the supplemental materials. During training, dropout with probability of 0.25 is applied to the output weights.

It should be noted that despite inheriting the neighborhood size parameter from traditional PCA, it is possible for a network trained on a specific k to be applied for other k as well, and that generalization across different k only leads to a very small increase in average error. This is because all networks can be shared across an arbitrary number of points and the softmax function normalizes weights for neighborhoods of varying sizes. However, to fairly evaluate our method for different k , a network is trained for each $k \in \{32, 48, 64, 96, 128\}$. Trained consists of 300 epochs using the RMSProp optimization method. All reported test results are given after 4 re-weighting iterations of our algorithm. Iterating longer does not show significant improvements. Quantitative results over iterations are presented in the supplemental materials. For details, we refer to our implementation, which we will make available online.

5.3. Quantitative Evaluation

RMSE results for the PCPNet test set of our approach (with $k = 64$) and related works are shown in Table 1. We

Neighborhood size k	Ours					PCA				
	32	48	64	96	128	32	48	64	96	128
No noise	6.09	6.63	6.72	6.82	7.35	9.10	9.94	10.68	11.93	12.54
Noise ($\sigma = 0.00125$)	10.22	9.63	9.95	10.45	9.64	11.22	11.56	12.08	12.71	12.97
Noise ($\sigma = 0.006$)	18.17	17.36	17.18	17.03	16.90	28.41	23.00	20.68	18.81	18.12
Noise ($\sigma = 0.012$)	25.17	22.40	21.96	21.80	22.13	45.35	38.48	33.67	28.81	26.67
Density (Stripes)	7.22	7.63	7.73	7.87	8.67	10.48	11.40	12.07	13.18	14.07
Density (Gradients)	6.84	7.19	7.51	7.69	8.49	9.96	10.74	11.35	12.36	13.21
Average	12.28	11.81	11.84	11.94	12.20	19.09	17.52	16.75	16.30	16.26

Table 2: Comparison of unoriented normal estimation RMSE between the proposed method and PCA for different neighborhood sizes k . It can be seen that our method consistently provides lower errors while being significantly more robust to changes of that parameter, compared to PCA.

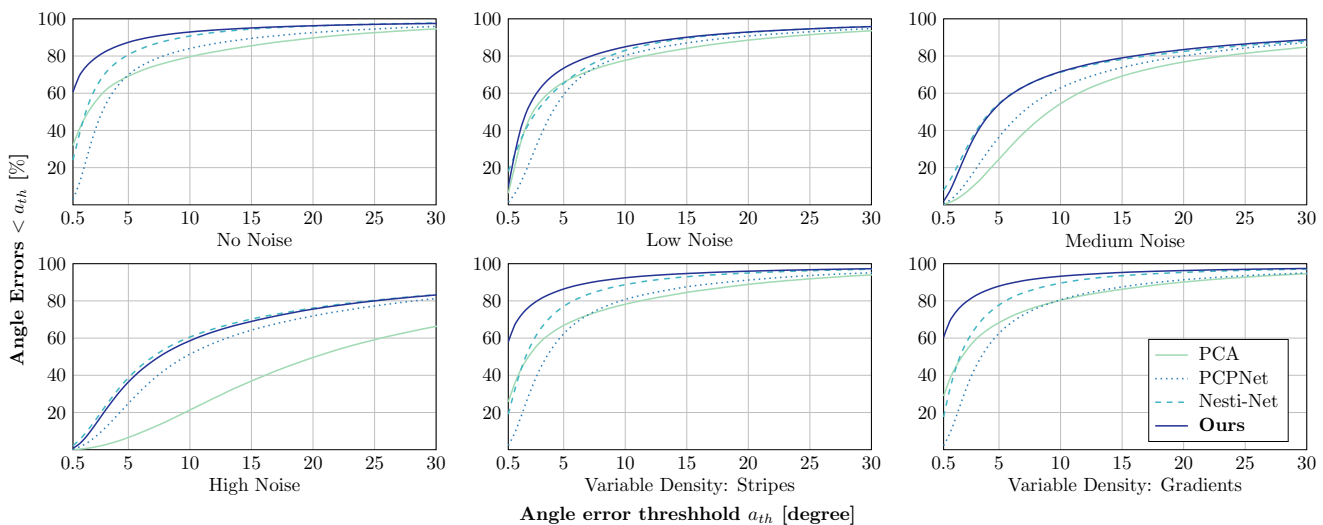


Figure 3: Comparison between methods for varying angle error threshold. For error thresholds on the x-axis, the y-axis shows the percentage of normals which have an error lower than that threshold. Our method and PCA use neighborhood size $k = 64$. For low noise settings and varying density, our method succeeds in recovering sharp features, as shown by the higher accuracies for low angle thresholds.

slightly improve on the state of the art on all noise levels and varying densities. For the non deep learning approaches, PCA and Jet, results for medium neighborhood sizes are displayed. In addition, results for different k are provided in Table 2 and compared to errors obtained by PCA with the same neighborhood sizes. Our method clearly outperforms the PCA baseline in all scenarios. As expected, varying k leads to a behavior similar to that of PCA, with large k 's performing better on more noisy data. However, it can be observed that our approach is more robust to changes of k : Even for small neighborhood sizes, high noise is handled significantly better than by PCA and large neighborhoods still produce satisfactory results for low noise data. It should be noted that for all evaluated k we improve on the state of the art w.r.t. average error.

While the RMSE error metric is well suited for a general comparison, it is not a good proxy to estimate the ability of recovering sharp features since it does not take into account the error distribution. Therefore, as an additional metric, Figure 3 presents the percentage of angle errors falling below different angle thresholds. The results confirm that our approach is better at preserving details and sharp edges, especially for low noise point clouds and varying density, where it outperforms other approaches. For higher noise, results similar to Nesti-Net are achieved.

5.4. Qualitative Evaluation

This section visually presents surface normal errors for various elements of the PCPNet test set in Figure 4 and compares them against results from the PCA baseline and

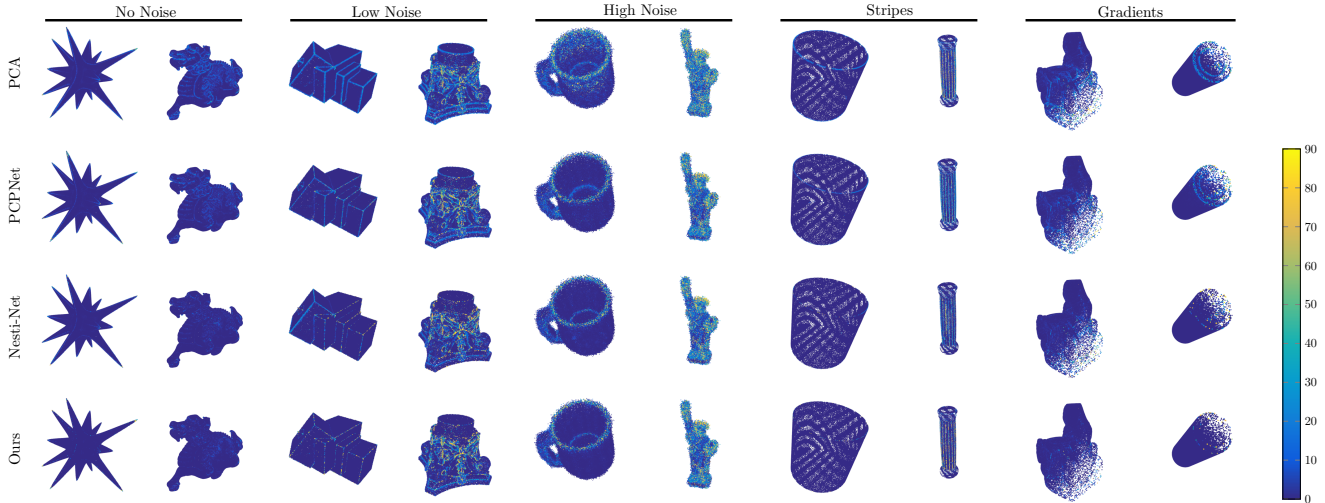


Figure 4: Qualitative comparison between our method ($k = 64$) and related work. We show diverse examples from the test set, sampled from different categories, noise levels and density variations. The color encodes the angle error of estimated normals in degrees. Best viewed in the digital version of the paper.

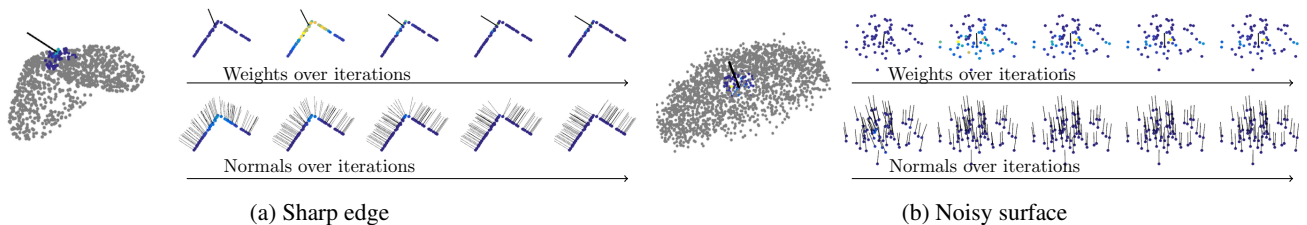


Figure 5: Local behaviour of our method over several iterations for a sharp edge (a) and a noisy surface (b). The partial point clouds were sampled from the PCPNet test dataset. The colors in the first rows show the weights from the kernel network for one normal in the neighborhood while the colors in the second row show the angle error of all neighborhood normals.

related deep learning approaches. It can be seen that the biggest improvements are obtained for low noise scenarios and varying density, where our method is able to preserve sharp features of objects better than the other methods. In general it can be observed that our approach tends to provide sharp, discriminative normals for points on edges instead of smooth averages. In rare cases, this can lead to a false assignment of points to planes, as we can see in the example in column 8. It is also worth mentioning that compared to Nesti-Net our approach behaves equivariant to input rotation as is seen nicely on the diagonal edge of the box example in column 3. Sharp edges are kept also in uncommon rotations, which we attribute to our local spatial transformer. Results for more examples are displayed in the supplemental material.

Interpretability. In order to interpret the results of our method, Figure 5 shows a detailed view of local neighborhoods over several iterations of our algorithm. An example

for a sharp edge is shown in Figure 5a and a high noise surface in Figure 5b. Both sets of points were sampled from the real test data. For the sharp edge, the algorithm initially fits a plane with uniform weights, leading to smoothed normals. Over the iterations, high weights concentrate on the more plausible plane, leading to recovering of the sharp edge. In the noisy example, we can see that outliers are iteratively receiving lower weights, leading to more stable estimates.

Surface reconstruction. To further evaluate the quality of the produced normals when used as input to other computer vision pipelines, Figure 6 shows the results for Poisson surface reconstruction. For this experiment, the normal signs are determined using the ground truth normals. Most of the point clouds do not show substantial differences, with our approach and Nesti-Net retaining slightly more details than the others. Significant differences can be observed for point clouds with varying density, displayed in rows 2 and 3. Here, our approach successfully retains the original structure of the object while still providing sharp edges.

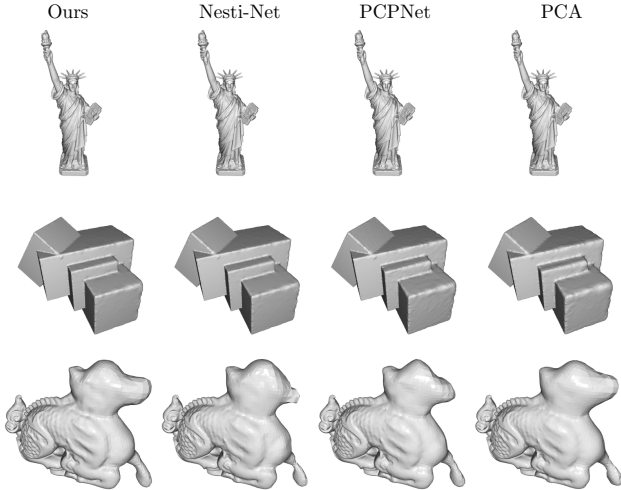


Figure 6: Selected results after applying Poisson surface reconstruction using the estimated normal vectors. In most cases, differences between the methods are very small. Examples 2 and 3 show reconstructions from point clouds with varying density, which show the largest differences.

Transfer to NYU depth dataset. In order to show generality of our approach, our models trained on the PCPNet dataset are validated on the NYU depth v2 dataset [35], a common benchmark dataset in the field of estimating normals from single images. It contains 1449 aligned and pre-processed RGBD frames, which are transformed to a point cloud before applying our method. After performing un-oriented estimation, the normals are flipped towards the camera position. Evaluation is done qualitatively, since the dataset does not contain ground truth normal vectors. Results for three different neighborhood sizes in comparison to PCA are shown in Figure 7. Our approach behaves as expected, as it is able to infer plausible normals for the given scenes. For all k , our approach is able to preserve sharp features while PCA produces very smooth results. However, this also leads to the sharp extraction of scanning artifacts, which can be seen on the walls of the scanned room.

5.5. Complexity

Our model is small, consisting of only 7981 trainable parameters, shared over iterations and spatial locations. On a single Nvidia Titan Xp, a point cloud with $100k$ points is processed in 5.67 seconds (0.0567 ms per point). The bottleneck of our method is the kd-tree used to compute the nearest neighbor graph, that takes 3.12 seconds of the 5.67 seconds. It is run on the CPU and could be greatly sped-up by utilizing GPUs. While Nesti-Net produces high-quality results similar to ours, it relies on heavy preprocessing of the point clouds, including a feature extraction procedure. Depending on the chosen model, Nesti-Net takes at least 1.5 minutes to process a point cloud with $100k$ points since

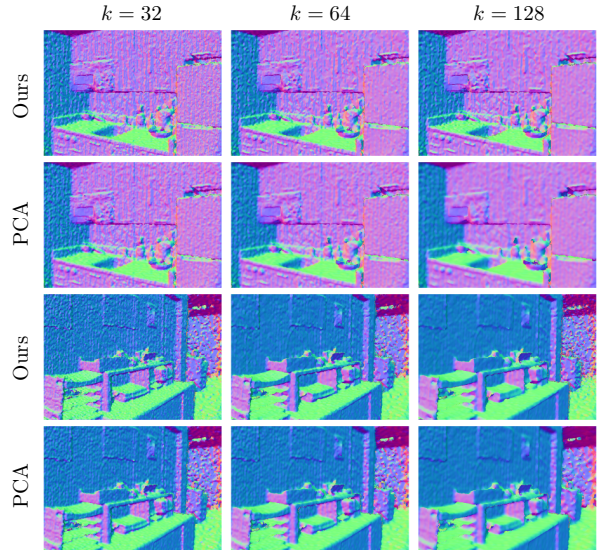


Figure 7: Examples for normal estimation on scanned data from the NYU depth v2 dataset. Colors encode the orientation of normals. Our model generalizes to this dataset while being able to retain more details and sharper edges than PCA. However, scanning artifacts are also kept and clearly visible. Best viewed in the digital version of the paper.

it needs to compute the input features for each neighborhood individually [4]. PCPNet is slightly faster, requiring approximately 1 minute. It should be noted that this is not a fair comparison as we can only compare unequally optimized implementations, provided by the respective authors. Nevertheless, it indicates that our approach scales better to large input sizes and is feasible for applications where faster estimation is required.

6. Conclusion

We presented a differentiable plane fitting algorithm for surface normal estimation on unstructured point clouds that uses backpropagation to compute gradients through eigenvector decomposition. Those gradients are used to train a deep neural network that iteratively refines the weights for the least squares problem. The algorithm is efficient and reaches state-of-the-art accuracy while being robust to parameter changes and interpretable. In the future we plan to further investigate the possibility of computing gradients through least squares problems. We suspect that introducing deep data-dependency to other traditional methods can also lead to progress in other fields of research, by reducing common disadvantages of pure deep learning approaches.

Acknowledgements

We thank Matthias Fey for his work on Pytorch Geometric. We also thank him and Prof. Dr. Heinrich Müller for helpful advice and discussions.

References

- [1] P. Alliez, D. Cohen-Steiner, Y. Tong, and M. Desbrun. Voronoi-based variational reconstruction of unoriented point sets. In *Proceedings of the Fifth Eurographics Symposium on Geometry Processing*, SGP '07, pages 39–48, 2007.
- [2] N. Amenta and M. Bern. Surface reconstruction by voronoi filtering. In *Proceedings of the Fourteenth Annual Symposium on Computational Geometry*, SCG '98, pages 39–48, 1998.
- [3] A. Bansal, B. C. Russell, and A. Gupta. Marr revisited: 2d-3d alignment via surface normal prediction. In *IEEE Conference on Computer Vision and Pattern Recognition (CVPR)*, pages 5965–5974, 2016.
- [4] Y. Ben-Shabat, M. Lindenbaum, and A. Fischer. Nestinet: Normal estimation for unstructured 3d point clouds using convolutional neural networks. *CoRR*, abs/1812.00709, 2018.
- [5] A. Boulch and R. Marlet. Fast and Robust Normal Estimation for Point Clouds with Sharp Features. *Computer Graphics Forum*, 2012.
- [6] A. Boulch and R. Marlet. Deep Learning for Robust Normal Estimation in Unstructured Point Clouds. *Computer Graphics Forum*, 2016.
- [7] M. M. Bronstein, J. Bruna, Y. LeCun, A. Szlam, and P. Vandergheynst. Geometric deep learning: Going beyond euclidean data. *IEEE Signal Processing Magazine*, 34(4):18–42, July 2017.
- [8] F. Cazals and M. Pouget. Estimating differential quantities using polynomial fitting of osculating jets. In *Proceedings of the 2003 Eurographics/ACM SIGGRAPH Symposium on Geometry Processing*, pages 177–187, 2003.
- [9] H. Deng, T. Birdal, and S. Ilic. Ppf-foldnet: Unsupervised learning of rotation invariant 3d local descriptors. In *European Conference of Computer Vision (ECCV)*, pages 620–638, 2018.
- [10] H. Deng, T. Birdal, and S. Ilic. Ppfnet: Global context aware local features for robust 3d point matching. In *IEEE Conference on Computer Vision and Pattern Recognition (CVPR)*, pages 195–205, 2018.
- [11] D. Eigen and R. Fergus. Predicting depth, surface normals and semantic labels with a common multi-scale convolutional architecture. In *Proceedings of the 2015 IEEE International Conference on Computer Vision (ICCV)*, pages 2650–2658, 2015.
- [12] M. Fey and J. E. Lenssen. Fast graph representation learning with PyTorch Geometric. *CoRR*, abs/1903.02428, 2019.
- [13] M. Fey, J. E. Lenssen, F. Weichert, and H. Müller. Splinecnn: Fast geometric deep learning with continuous b-spline kernels. In *IEEE Conference on Computer Vision and Pattern Recognition (CVPR)*, pages 869–877, 2018.
- [14] D. F. Fouhey, A. Gupta, and M. Hebert. Data-driven 3D primitives for single image understanding. In *International Conference on Computer Vision (ICCV)*, 2013.
- [15] M. B. Giles. Collected matrix derivative results for forward and reverse mode algorithmic differentiation. In C. H. Bischof, H. M. Bücker, P. Hovland, U. Naumann, and J. Utke, editors, *Advances in Automatic Differentiation*, pages 35–44. Springer Berlin Heidelberg, 2008.
- [16] E. Grilli, F. Menna, and F. Remondino. A review of point clouds segmentation and classification algorithms. *ISPRS - International Archives of the Photogrammetry, Remote Sensing and Spatial Information Sciences*, XLII-2/W3:339–344, 02 2017.
- [17] G. Guennebaud and M. Gross. Algebraic point set surfaces. *ACM Transactions on Graphics*, 26(3), 2007.
- [18] P. Guerrero, Y. Kleiman, M. Ovsjanikov, and N. J. Mitra. Pcpnet learning local shape properties from raw point clouds. *Computer Graphics Forum*, 37(2):75–85, 2018.
- [19] W. L. Hamilton, Z. Ying, and J. Leskovec. Representation learning on graphs: Methods and applications. *IEEE Data Eng. Bull.*, 40:52–74, 2017.
- [20] R. Hartley and A. Zisserman. *Multiple View Geometry in Computer Vision*. Cambridge University Press, New York, NY, USA, 2 edition, 2003.
- [21] H. Hoppe, T. DeRose, T. Duchamp, J. McDonald, and W. Stuetzle. Surface reconstruction from unorganized points. In *Proceedings of the 19th Annual Conference on Computer Graphics and Interactive Techniques, SIGGRAPH '92*, pages 71–78, 1992.
- [22] H. Huang, S. Wu, M. Gong, D. Cohen-Or, U. Ascher, and H. R. Zhang. Edge-aware point set resampling. *ACM Trans. Graph.*, 32(1):9:1–9:12, Feb. 2013.
- [23] X. Huang, Z. Liang, X. Zhou, Y. Xie, L. J. Guibas, and Q. Huang. Learning transformation synchronization. *CoRR*, abs/1901.09458, 2019.
- [24] M. Jaderberg, K. Simonyan, A. Zisserman, and K. Kavukcuoglu. Spatial transformer networks. In *Proceedings of the 28th International Conference on Neural Information Processing Systems (NeurIPS)*, pages 2017–2025, 2015.
- [25] M. Kazhdan, M. Bolitho, and H. Hoppe. Poisson surface reconstruction. In *Proceedings of the Fourth Eurographics Symposium on Geometry Processing*, SGP '06, pages 61–70, 2006.
- [26] K. Klasing, D. Althoff, D. Wollherr, and M. Buss. Comparison of surface normal estimation methods for range sensing applications. In *2009 IEEE International Conference on Robotics and Automation*, pages 3206–3211, May 2009.
- [27] L. Ladicky, B. Zeisl, and M. Pollefeys. Discriminatively trained dense surface normal estimation. In *ECCV*, 2014.
- [28] D. Levin. The approximation power of moving least-squares. *Math. Comput.*, 67(224):1517–1531, Oct. 1998.
- [29] B. Li, C. Shen, Y. Dai, A. van den Hengel, and M. He. Depth and surface normal estimation from monocular images using regression on deep features and hierarchical crfs. In *2015 IEEE Conference on Computer Vision and Pattern Recognition (CVPR)*, pages 1119–1127, 2015.
- [30] J. Masci, D. Boscaini, M. M. Bronstein, and P. Vandergheynst. Geodesic convolutional neural networks on riemannian manifolds. In *Proceedings of the 2015 IEEE International Conference on Computer Vision Workshop (ICCVW)*, pages 832–840, 2015.

- [31] Q. Merigot, M. Ovsjanikov, and L. J. Guibas. Voronoi-based curvature and feature estimation from point clouds. *IEEE Transactions on Visualization and Computer Graphics*, 17(6):743–756, 2011.
- [32] N. J. Mitra, A. Nguyen, and L. Guibas. Estimating surface normals in noisy point cloud data. In *special issue of International Journal of Computational Geometry and Applications*, volume 14, pages 261–276, 2004.
- [33] F. Monti, D. Boscaini, J. Masci, E. Rodolà, J. Svoboda, and M. M. Bronstein. Geometric deep learning on graphs and manifolds using mixture model cnns. In *IEEE Conference on Computer Vision and Pattern Recognition (CVPR)*, pages 5425–5434, 2017.
- [34] C. Morris, M. Ritzert, M. Fey, W. L. Hamilton, J. E. Lenssen, G. Rattan, and M. Grohe. Weisfeiler and leman go neural: Higher-order graph neural networks. In *AAAI Conference on Artificial Intelligence (AAAI)*, 2019.
- [35] P. K. Nathan Silberman, Derek Hoiem and R. Fergus. Indoor segmentation and support inference from rgb-d images. In *European Conference on Computer Vision (ECCV)*, 2012.
- [36] F. Pomerleau, F. Colas, and R. Siegwart. A review of point cloud registration algorithms for mobile robotics. *Found. Trends Robot.*, 4(1):1–104, May 2015.
- [37] C. R. Qi, L. Yi, H. Su, and L. J. Guibas. Pointnet++: Deep hierarchical feature learning on point sets in a metric space. In *Advances in Neural Information Processing Systems 30*, pages 5099–5108. 2017.
- [38] X. Qi, R. Liao, Z. Liu, R. Urtasun, and J. Jia. Geonet: Geometric neural network for joint depth and surface normal estimation. *IEEE Conference on Computer Vision and Pattern Recognition (CVPR)*, pages 283–291, 2018.
- [39] M. Rakotosaona, V. L. Barbera, P. Guerrero, N. J. Mitra, and M. Ovsjanikov. POINTCLEANNET: learning to denoise and remove outliers from dense point clouds. *CoRR*, abs/1901.01060, 2019.
- [40] R. Ranftl and V. Koltun. Deep fundamental matrix estimation. In *European Conference on Computer Vision (ECCV)*, September 2018.
- [41] S. Suwajanakorn, N. Snavely, J. J. Tompson, and M. Norouzi. Discovery of latent 3d keypoints via end-to-end geometric reasoning. In *Advances in Neural Information Processing Systems 31: Annual Conference on Neural Information Processing Systems (NeurIPS)*, pages 2063–2074, 2018.
- [42] X. Wang, D. F. Fouhey, and A. Gupta. Designing deep networks for surface normal estimation. *2015 IEEE Conference on Computer Vision and Pattern Recognition (CVPR)*, pages 539–547, 2015.

Supplemental Materials

The supplemental materials contain details about the graph neural network in Section 1, information about the implementation in Section 2, and an additional analysis of test error over re-weighting iterations in Section 3. Further, we show results for transferring models between different neighborhood sizes in Section 4 and qualitative results for the whole PCPNet test set in Section 5.

1. Architecture Details

The graph neural network for deep re-weighting consists of 7 MLPs in total, which are detailed in Table 3. For convenience, we provide the associated equations again. Six of the MLPs, h_i and γ_i for $i \in \{1, 2, 3\}$, belong to the three neighborhood aggregation layers, each given by

$$\mathbf{f}_e^{\text{out}}(i, j) = h(\mathbf{f}_e^{\text{in}}(i, j) \parallel \mathbf{d}_{i,j} \parallel \mathbf{ppf}(i, j)), \quad (15)$$

$$\mathbf{f}(i) = \gamma\left(\frac{1}{|\mathcal{N}(i)|} \sum_{j \in \mathcal{N}(i)} \mathbf{f}_e^{\text{out}}(i, j)\right). \quad (16)$$

The last MLP ψ computes the actual weights for the neighborhood by

$$(\mathbf{f}_{\mathcal{N}(i)}^{\text{par}}, \mathbf{q}_{\mathcal{N}(i)}) = \mathbf{f}(i), \quad (17)$$

$$w_{i,j} = \text{softmax}(\psi(\mathbf{f}_{\mathcal{N}(i)}^{\text{par}} \parallel \mathbf{R}(\mathbf{q}_{\mathcal{N}(i)})(\mathbf{p}_j - \mathbf{p}_i))). \quad (18)$$

The h_i and ψ networks are shared over all edges in the neighborhood graph while the γ_i are shared over all points. Additionally, all MLPs are shared over the iterations of the algorithm. Each MLP consists of two linear layers, separated by a ReLU non-linearity. Layer sizes are given in Table 3. All in all, the networks contain 7981 parameters and fulfill the following properties.

Network	Architecture
h_1	$L(32), \text{ReLU}, L(16)$
γ_1	$L(32), \text{ReLU}, L(8)$
h_2	$L(32), \text{ReLU}, L(16)$
γ_2	$L(32), \text{ReLU}, L(8)$
h_3	$L(32), \text{ReLU}, L(16)$
γ_3	$L(32), \text{ReLU}, L(12)$
ψ	$L(64), \text{ReLU}, L(1)$

Table 3: Details of the used graph neural network for iterative re-weighting. $L(x)$ stands for a fully-connected layer with x output neurons.

Permutation Invariance Neighborhood aggregation is performed using an average operator, which is invariant regarding the order of points. Since there are no other func-

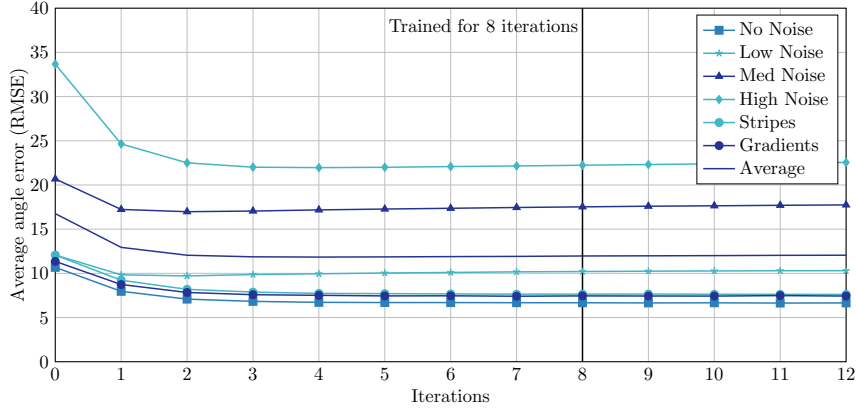


Figure 8: Test errors (RMSE) over iterations of the proposed algorithm. Iteration 0 shows results for unweighted PCA only. The network was trained on the training set for 8 iterations. For evaluation, we perform four additional iterations to evaluate stability.

k^{test}	Trained on $k^{\text{train}} = 32$					Trained on $k^{\text{train}} = 64$					Trained on $k^{\text{train}} = 128$				
	32	48	64	96	128	32	48	64	96	128	32	48	64	96	128
No noise	6.09	6.96	7.43	8.25	8.77	6.13	6.47	6.72	7.10	7.27	6.66	7.01	7.24	7.29	7.35
Noise ($\sigma = 0.00125$)	10.22	10.01	10.09	10.37	10.62	10.19	9.93	9.95	10.18	10.35	9.89	9.57	9.50	9.50	9.64
Noise ($\sigma = 0.006$)	18.17	17.44	17.22	17.08	17.05	18.28	17.43	17.18	17.01	16.94	20.98	18.40	17.63	17.07	16.90
Noise ($\sigma = 0.012$)	25.17	22.97	22.33	21.91	21.80	25.20	22.53	21.96	21.69	21.67	30.99	24.94	23.20	22.34	22.13
Density (Stripes)	7.22	7.92	8.51	9.43	9.90	7.21	7.55	7.73	8.16	8.34	7.80	8.14	8.37	8.61	8.67
Density (Gradients)	6.84	7.46	8.06	8.80	9.21	6.89	7.17	7.51	8.04	8.03	7.48	7.75	8.11	8.39	8.49
Average	12.28	12.12	12.27	12.64	12.89	12.31	11.85	11.84	12.00	12.10	13.97	12.63	12.34	12.20	12.20

Table 4: Results for transferring models between different neighborhood sizes k . Shown are RMSE values for models trained with $k^{\text{train}} \in \{32, 64, 128\}$, each tested with $k^{\text{test}} \in \{32, 48, 64, 96, 128\}$.

tions over sets of points, the resulting network is permutation invariant. We refer to [37] for further discussion.

Varying neighborhood sizes For the cases in which we decide to use a radius graph instead of a k-nn graph, the network allows differently sized neighborhoods in one graph, since all parameters are shared over edge or nodes and the only operation over the whole neighborhood, the average, is agnostic to the neighborhood size.

Constant receptive field Due to how the edge input features $\mathbf{f}_e^{\text{in}}(i, j) = (\mathbf{f}_e^{\text{out}}(i, j) \parallel \mathbf{f}(i))$ are computed for the second and third aggregation layers, the network has a constant receptive field: the neighborhood $\mathcal{N}(i)$. We do not obtain features from node j , which would be usually done in message passing schemes on graphs.

Note that due to the constant receptive field, the presented algorithm can be applied locally, without the need of extracting larger neighborhoods around a point for which a normal vector should be computed.

2. Implementation Details

The implementation of the proposed algorithm is based on the *Pytorch Geometric* library [12] and uses the provided scheme consisting of scattering and gathering between node and edge feature space. Therefore, varying neighborhood sizes (e.g. varying node degree) can still be handled in parallel on the GPU by parallelization in graph edge space.

For parallel eigendecomposition of a large number of symmetric 3×3 matrices, we provide our own Pytorch extension which will be made available online. We provide efficient forward and backward steps on GPU and CPU.

3. Behaviour over iterations

The network is trained for $L = 8$ (performing 8 iterations of re-weighting), where we compute a loss and perform an optimization step after each iteration. The algorithm produces normal vector estimations after each iteration, which can be analyzed quantitatively. The RMSE results for the PCPNet test set over algorithm iterations are shown in Figure 8. It can be seen that after iteration 4,

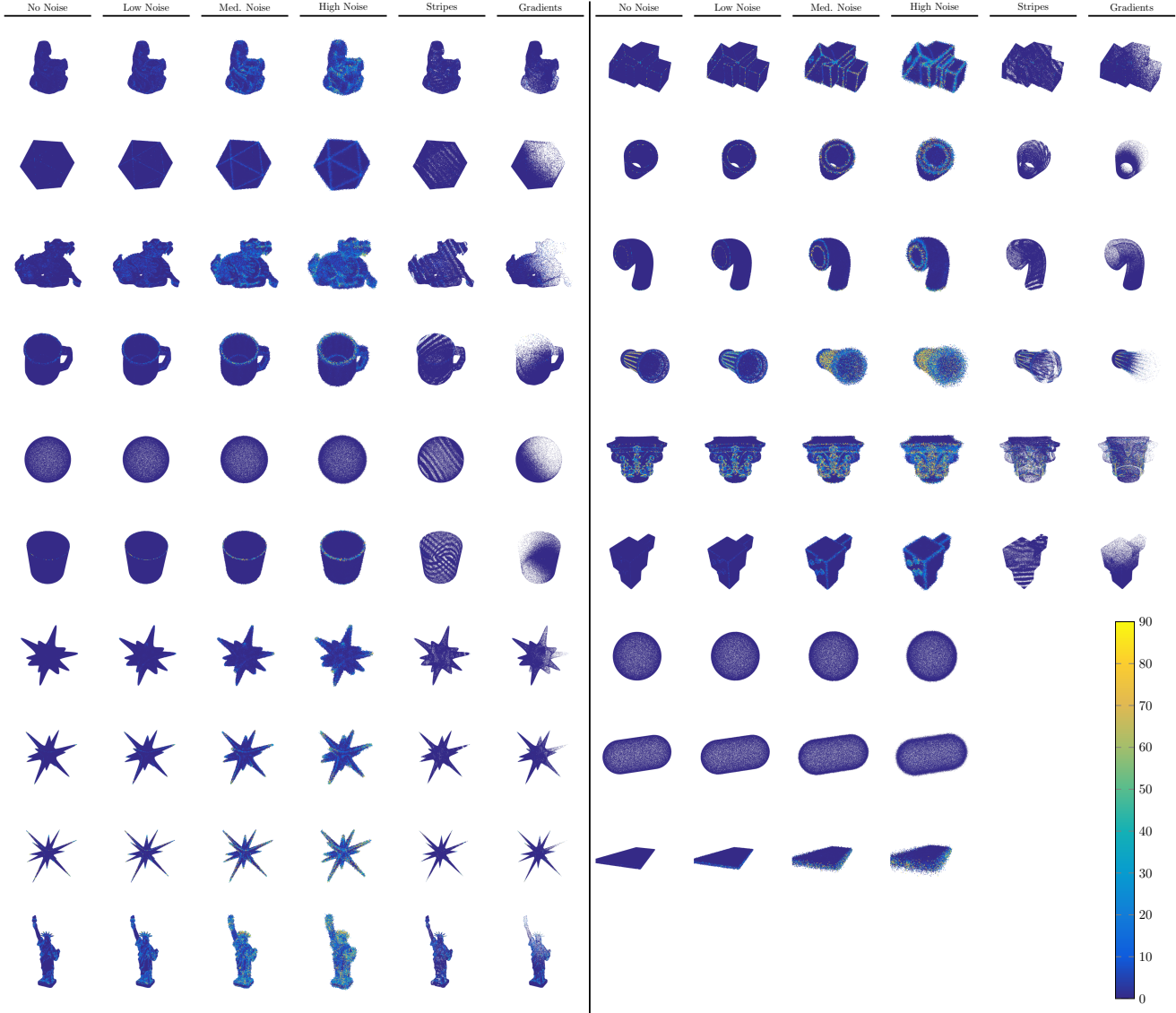


Figure 9: Qualitative results for all examples of the test set. Colors encode the RMSE in degree for each point. Best viewed in the digital version.

further iterations do not lead to significant improvements. Also, the algorithm behaves reasonable stable, not diverging immediately after we pass the iterations for which the network was trained. However, we observe a small drift in favor of low-noise datasets over the iterations. Errors for the test sets with no noise or variable density still decrease further while errors for data with higher noise levels slightly increase. Meanwhile, the average error stays nearly constant.

4. Transfer between neighborhood sizes

As stated in the main paper, the proposed algorithm generalizes reasonably well between neighborhood sizes,

meaning that a model trained using neighborhood size k^{train} can be applied using a different neighborhood size k^{test} while producing good results. For verification, we report RSME errors for different combinations of k^{train} and k^{test} in Table 4. It can be seen that if the difference in neighborhood size is not too big, transferred models often only perform slightly worse than models trained directly for the appropriate k . However, transferring over very large difference like from 128 to 32 or the other way around, leads to a significant decrease in performance. The model trained on the balanced $k = 64$ performs very well on all other neighborhood sizes. Note that it is also possible to train the network using varying and randomly sampled neighborhood sizes. Evaluation of this scenario is left for future work.

5. Further qualitative results

Last, we provide qualitative results for the whole PCP-Net test set in Figure 9. For point clouds with varying density, the point size is reduced in order to better visualize the densities. Similar to examples shown in the paper, we can see that the method produces very sharp normal vectors, which usually resemble the plane normal of one of the plausible planes in the neighborhood. Sometimes, points are assigned to a false plane, leading to high error normal vectors. Compared to other approaches, we do not observe heavy smoothing around edges.